Materials Research. 2025; 28: e20250398
DOI: https://doi.org/10.1590/1980-5373-MR-2025-0398

Microstructure, Optical Properties, and Dielectric Properties of Film Ceramics $BaTiO_3$–$BaZr_{0.5}Ti_{0.5}O_3$ for High-Temperature Capacitors

***Rahmi Dewi*[a]*, *Lulu Hayati*[a], *Faiza Fadhila*[a], *Zulfa Nasir*[a], *Ari Sulistyo Rini*[a], *Yanuar Hamzah*[a]**

[a]*University of Riau, Faculty of Mathematics and Natural Sciences, Department of Physics, Pekanbaru, Indonesia.*

Received: April 02, 2025; Revised: July 04, 2025; Accepted: July 08, 2025

Ceramics composed of $(0.1)BaTiO_3$–$(0.9)BaZr_{0·5}Ti_{0·5}O_3$ have been synthesized to fulfill the specifications required for multilayer ceramic capacitors. This study investigates the influence of various annealing temperatures on the materials' microstructure, optical properties, and dielectric characteristics. Findings indicate that elevated annealing temperatures enhance crystallinity, grain size, dielectric constant, and capacitance. Notably, samples annealed at 800 °C demonstrate high crystallinity, increased grain size, a reduced energy band gap (Eg ≈ 3.50 eV), an optimal dielectric constant of approximately 80,000, and a dielectric loss tangent (tan δ) of about 0.14 at room temperature. The substantial dielectric constant suggests that these capacitors are capable of operating effectively at high temperatures. Furthermore, at a frequency of 100 Hz, capacitance values rise with increasing annealing temperature, reaching approximately 70 μF at 800 °C. These results propose that this material holds significant promise as a candidate for high-temperature multilayer ceramic capacitors.

Keywords: *Microstructure, Energy band gap, Dielectric constant, Capacitance.*

1. Introduction

There is now a much greater need for high-performance electronic components that can function in harsh environments, like those found in oil drilling, automotive, and aerospace applications. In these systems, multilayer ceramic capacitors (MLCCs) are crucial, however because of temperature-dependent dielectric constants, traditional dielectric materials like $BaTiO_3$ (BT) find it difficult to maintain thermal reliability over 150 °C[1,2]. BT-based solid solutions have been extensively studied to get around this restriction by adding dopants or creating new composite systems like $BaTiO_3$–$(Bi_{0·5}Na_{0·5})TiO_3$ (BT–BNT), $BaTiO_3$–$Ba(Zn_{0·5}Ti_{0·5})O_3$, and $BaTiO_3$–$Bi(Mg_{0·5}Zr_{0·5})O_3$[3]. Among these, the BT–BNT system has demonstrated potential for X9R-class MLCCs, particularly upon achieving optimal dopant gradients and a fine-grained core-shell structure[4].

The substitution of Zr^{4+} for Ti^{4+} in the BT lattice (creating $BaTiO_3$–$BaZr_{0·5}Ti_{0·5}O_3$ or BT–BZT) has been emphasized in recent studies as an efficient way to improve resistance to electric field degradation, boost microstructural densification, and improve thermal stability[5,6]. Additionally, BT–BZT ceramics have advantageous ferroelectric and dielectric characteristics, which make them desirable for application in transducers, sensors, and MLCCs[7,8].

A semiconductor material with ferroelectric characteristics, barium titanium-barium zirconium titanate (BT-BZT) is distinguished by discrete valence and conduction bands that are separated by an energy band gap (Eg). One important component of its electrical structure is the Eg value, which varies based on the production pathway or processing technique used. For applications in materials science and engineering, it is crucial to calculate Eg accurately[9]. The potential of BT-BZT as a high-temperature-resistant sensor is examined in this work.

Holding time—the amount of time a sample stays at a particular temperature in a furnace—and annealing temperature are two variables that affect grain size in materials. Grain interactions during this time cause diffusion processes, which in turn cause grain expansion. Grain size increases in BT-BZT ceramics have been linked to improved ferroelectric characteristics, such as reduced coercive electric field and greater remanent polarization[10].

By changing and holding the annealing temperature for an hour, this study investigates the function of the annealing temperature in the BT-BZT system. It also takes into account how changes in annealing temperature affect the electrical, optical, and microstructure characteristics relevant to high-temperature applications. By developing novel materials with small grains, controlled doping gradients, and increased resistance to high temperatures, the invention focuses on deploying X9R high-temperature multilayer ceramic capacitors (MLCCs). Appropriate variations in annealing and doping temperatures can be applied to various types of sensors[11].

2. Experiment Procedure

The BT-BZT sample was prepared using the sol-gel method. Two solutions, BT and BZT, were used. The BT solution was formulated by adding and stirring 0.1 M $BaCO_3$ solution into 0.1 M TiO_2 solution. The $BaCO_3$ solution was created by mixing $BaCO_3$ powder with 80% acetic acid

*e-mail: drahmi2002@yahoo.com
Associate Editor: Jose Eiras.
Editor-in-Chief: Luiz Antonio Pessan.

and 20% deionized water. This mixture was subsequently stirred using a hotplate with a magnetic stirrer. The TiO_2 dispersion was prepared by dispersing TiO_2 powder in 96% ethanol. A 0.6 ml and 0.4 ml of 10% ethylene glycol were subsequently added, and the resulting mixture was stirred thoroughly using a hotplate with a magnetic stirrer to achieve a fully blended solution.

The BZT solution was a mixture of ZrO_2 and TiO_2 powder with 80% acetic acid and 20% deionized water. Ba powder was added to 10 ml of this solution, and the mixture was stirred on a hotplate until a transparent solution was obtained. The BT/BZT sample was then created by mixing the BT and BZT solutions. This mixed solution was stabilized by adding 3 drops of acetyl acetone and stirring until its color turned yellowish clear.

A thin layer was created using the spin-coating method by applying 3 drops of BT-BZT solution onto the fluorine tin oxide (FTO) substrate placed on the spin coater. The thin layer then underwent an annealing process in a furnace at temperatures of 700 °C, 750 °C, and 800 °C. This temperature was maintained for 1 hour. The purpose of this annealing process was to induce a crystalline structure in the BT-BZT thin films. The samples were then characterized using XRD, FESEM, UV-Vis, and impedance spectroscopy.

The optical absorption of the synthesized $(0.1)BaTiO_3$–$(0.9)BaZr_{0.5}Ti_{0.5}O_3$ sample was analyzed using a UV-Vis spectrophotometer (LAMBDA 35, Perkin Elmer, USA). The results are presented as a lookup table of the absorbance spectrum as a function of wavelength (250-900 nm). Information on the crystal structures of the BT-BZT700, BT-BZT750, and BT-BZT800 samples was obtained using X-ray diffraction (XRD) characterization with Cu Kα radiation (λ = 1.54178 Å) on a D8 Advance instrument from Bruker Inc., Germany. The XRD scanning was performed over a 2-hour range from 10° to 70° (2θ), with a scanning speed set at 6°/min.

The surface morphology of the BT-BZT sample was evaluated using field-emission scanning electron microscopy (FESEM) (LEO VPSEM 1450 model). This FESEM characterization method provided insights into the shape and size of the particles present in the sample.

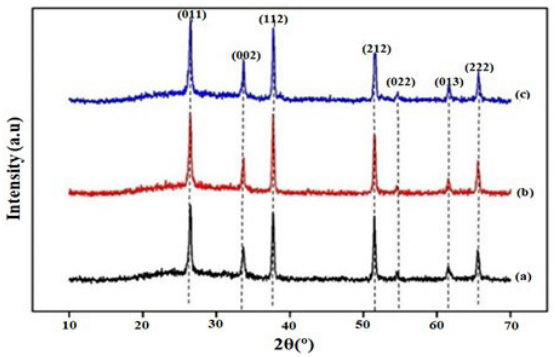

Figure 1. The pattern of XRD sample BT-BZT at the temperature of (a) 700 °C, (b) 750 °C, and (c) 800 °C

Impedance spectroscopy characterization was performed using the Solartron-Schlumberger 1255 model. This characteritazation was done to ascertain the electrical properties of the BT-BZT thin films, including the dielectric constant and capacitance. The procedure involved examinations of the correlation between the capacitance value and the logarithm of frequency, as well as the correlation between the dielectric constant and the logarithm of frequency. The measurements were conducted over a frequency range from 10 Hz to 1 MHz, with the alternating current voltage maintained at 0.5 volts.

3. Results and Discussion

Figure 1 shows X-ray diffraction (XRD) patterns at various annealing temperatures. The resulting X-ray diffraction pattern indicated that the BT-BZT sample had a tetragonal crystal structure[12], which is in good agreement with the Joint Committee on Powder Diffraction Standards (JCPDS) data (code 98-009-4258). The results of the XRD analysis revealed the lattice parameters and crystallite size. The intensity, crystallinity, and crystal size of the BT-BZT thin films exhibit an upward trend with increasing annealing temperatures. This is attributed to the higher temperature leading to greater atomic orderliness due to increased atomic vibrations[13].

The crystallite size (D) is calculated using the Debye-Scherrer method Equation 1.

$$D = \frac{k\lambda}{\beta cos} \tag{1}$$

where k is the proportionality constant (0.94), β is the full width at half maximum (FWHM) of the main peak in the X-ray diffraction, λ is the wavelength of the X-ray (1.548 nm for Cu-Kα), and θ is the diffraction angle. To determine the strain values of the thin film, the Williamson-Hall (W-H) method[14] was used, as described in Equation 2,

$$\frac{\beta cos\theta}{\lambda} = \frac{0.89}{D} + 4\varepsilon\frac{sin\theta}{\lambda} \tag{2}$$

where D represents the crystallite size, and ε denotes the strain. The strain values were then obtained from the slope of the plot of sin(θ)/ λ versus cos(θ)/ λ, in accordance with Equation 2, as shown in Figure 2.

The density of the thin films was calculated using Equation 3.

$$\rho = \frac{Z \cdot M}{a^2 \cdot c \cdot Na} \tag{3}$$

Where ρ is the density (g/cm^3) of BT-BZT, $Z = 4$, M is the molar mass of BT-BZT, $Na = 6.022 \times 10^{23}$/mol, and a and c are lattice constants. The specific surface area (SSA) of the composition was then estimated using Equation 4.

$$SSA = \frac{6 \cdot 10^3}{\rho \cdot D} \tag{4}$$

The obtained strain, lattice parameter, density, and SSA values are summarized in Table 1.

Figure 3 shows the FESEM micrograph of the BT-BZT sample, revealing particles with irregular spherical

shapes. The annealing process led to an increase in grain size, with the average values of 209.9 ± 14.5 nm, 224.4 ± 14.9 nm, and 253.2 ± 15.9 nm at annealing temperatures of 700, 750, and 800 °C, respectively. The annealing process significantly influences grain growth through mechanisms such as nucleation and recrystallization. Nucleation can occur in both solution and solid phases during annealing, while recrystallization generally takes place in the solid state. These processes enhance atomic mobility by increasing thermal vibrational energy, which promotes the migration of atoms across grain boundaries. As a result, smaller grains tend to merge with larger ones, and some may vanish entirely, contributing to overall grain coarsening[15].

Figure 4 shows that the BT-BZT sample contains the element Sn (tin), O (oxygen), C (carbon), Ba (barium), Ti (titanium), Zr (zirconium), and Si (silicon). Based on the Energy Dispersive X-ray (EDX) analysis, the BT-BZT700 sample exhibits weight percentages of 44.4% Sn, 41.2% O, 12.0% C, 1.0% Ba, 0.9% Ti, 0.3% Zr, and 0.2% Si. For the BT-BZT750 sample, the respective weight percentages are 72.3% Sn, 19.4% O, 7.9% C, 0.3% Ba, 0.1% Zr, 0.0% Ti, and 0.0% Si. Meanwhile, the BT-BZT800 sample contains 73.4% Sn, 22.1% O, 3.4% C, 0.8% Ba, 0.1% Zr, 0.0% Ti, and 0.0% Si. The EDX spectra indicate that Sn is the doimant element in all samples. This high Sn content originates from the FTO substrate, not from the BT-BZT

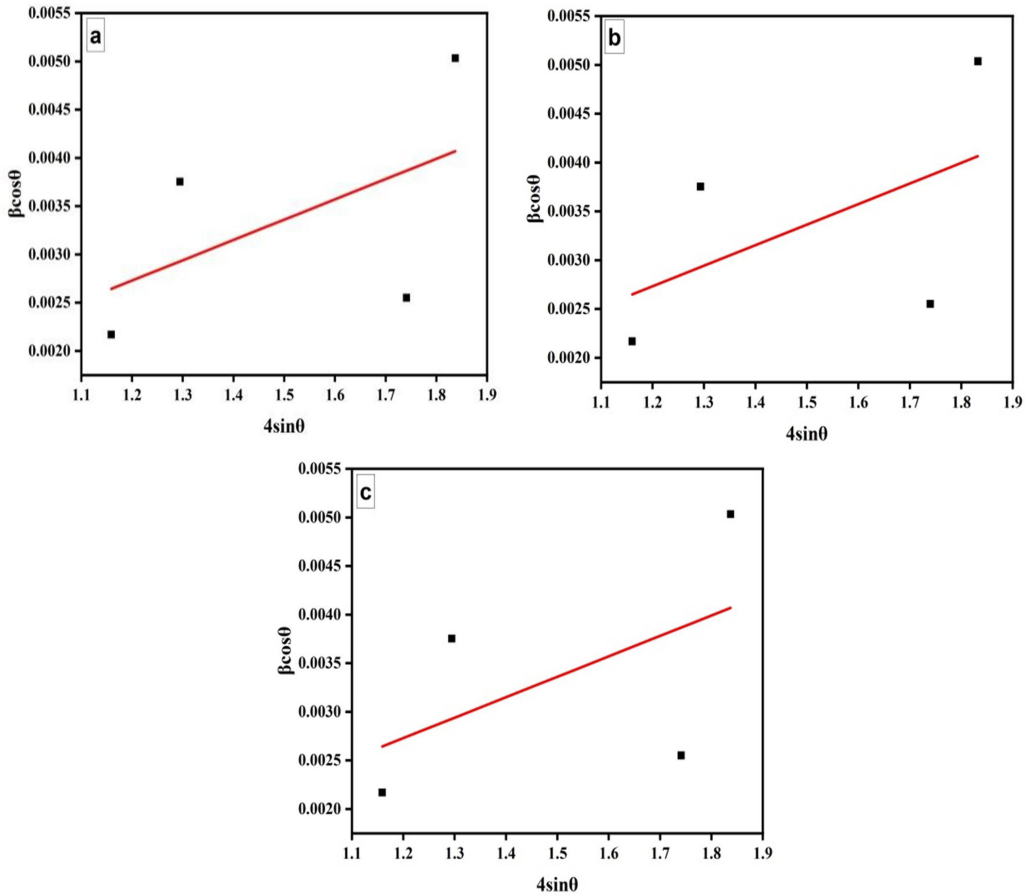

Figure 2. Williamson-Hall plot to estimate D and ε for BT-BZT (1.5 mol%) at (a) 700 °C, (b) 750 °C, and (c) 800 °C.

Table 1. XRD analysis.

Sample	Debye Scherrer D (nm)	W-H D (nm)	Strain (ε) $x10^{-3}$	a(Å)	c(Å)	c/a	ρ (g/cm³)	SSA (m^2/g)	Volume of unit cell (Å)³
BT-BZT700	7.78	7.37	2.1	3.39	4.98	1.48	3.06	252	57.23
BT-BZT750	7.81	7.42	2.1	4.25	5.64	1.32	3.30	232.7	106.0
BT-BZT800	7.87	7.48	2.1	4.78	15.96	3.36	4.81	158.4	364.66

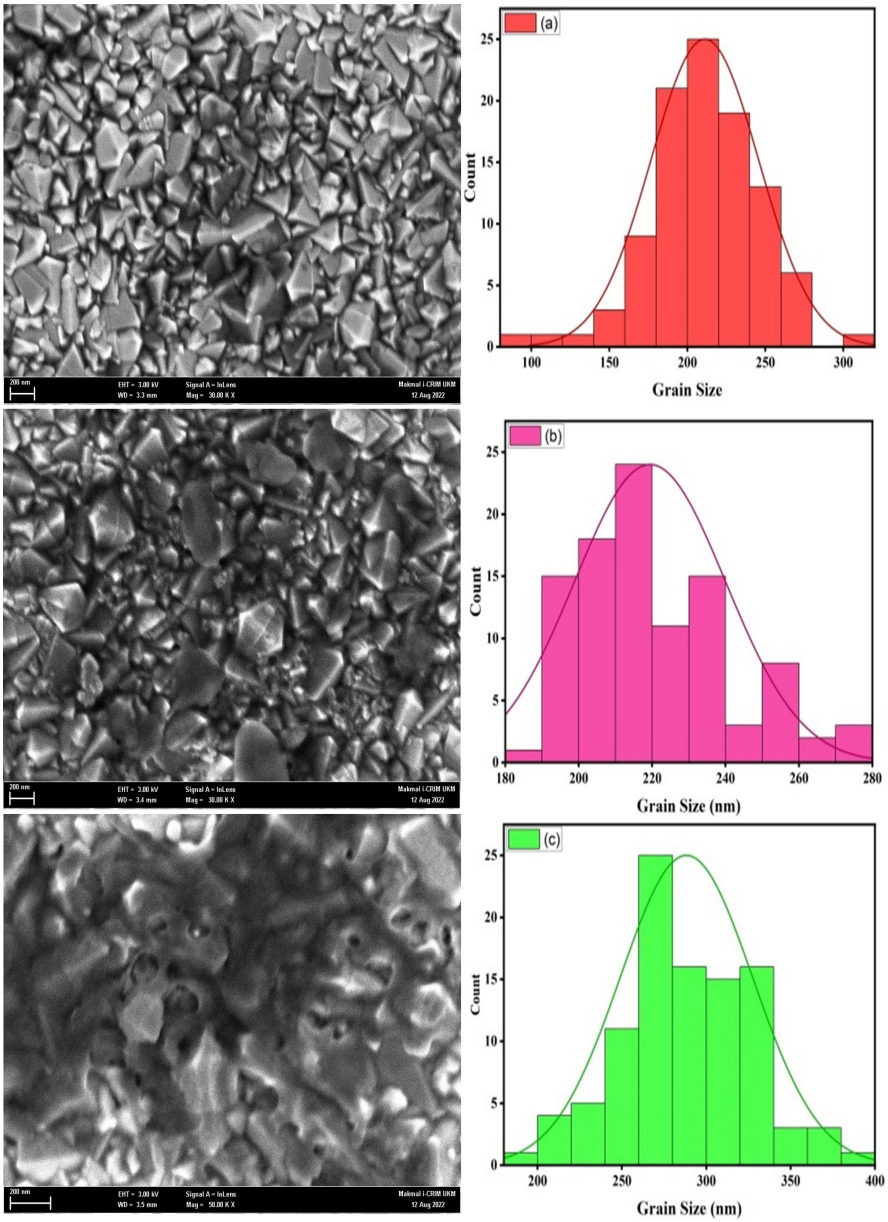

Figure 3. Photos of FESEM scans at annealing temperatures of (a) 700 °C, (b) 750 °C, and (c) 800 °C

material itself. Figure 5 further confirms that all the detected elements in the BT-BZT sample were uniformly distributed throughout the films[16]. The cross-sectionalview of the films also reveals that the thickness of the thin film above the FTO substrate is approximately 6.4 x 10^{-7} m.

Figure 6 shows the optical absorption peaks of the BT-BZT700, BT-BZT750, and BT-BZT800 samples, oberved at wavelengths of 311 nm, 309 nm, and 310 nm, respectively. These peaks in the UV region indicate the formation of BT-BZT particles. The optical absorption peak of approximately 310 nm corresponds to the electronic transition from the ground state to a higher energy state, typically associated with particle formation in semiconductor or ceramic materials like BT-BZT. This UV absorption suggests that the material begins to absorb photon energy in this range, and this likely due to bond formation between constituent elements. The slight differences in the wavelength of the absorption peak suggest variations in particle size or material composition at different annealing temperatures. This indicates that the processing temperature affects the size and distribution of the formed BT-BZT particles. The annealing process influences crystallization and grain growth, which in turn affects its optical properties[17].

Figure 6 also shows that higher annealing temperatures lead to higher absorbance values, with maximum absorbance observed at 700 °C (~0.0554 a.u.), 750 °C (~0.0952 a.u.), and 800 °C (~0.1121 a.u.). Across all samples, the absorbance decreased with increasing wavelengths, from the UV to the

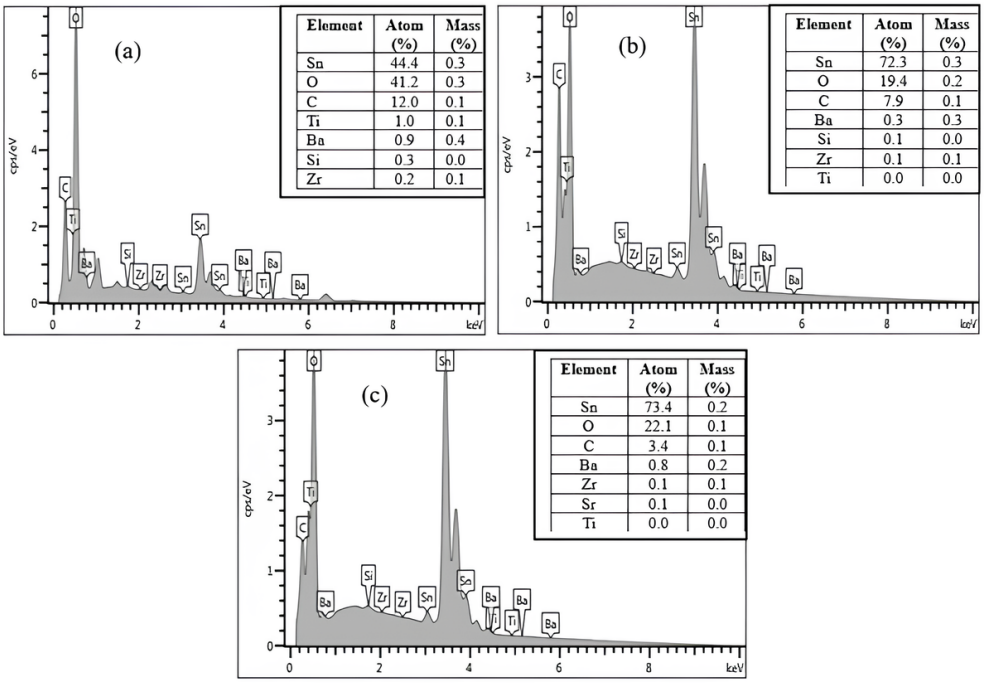

Figure 4. Results of the EDX spectrum at annealing temperatures of (a) 700 °C, (b) 750 °C, and (c) 800 °C.

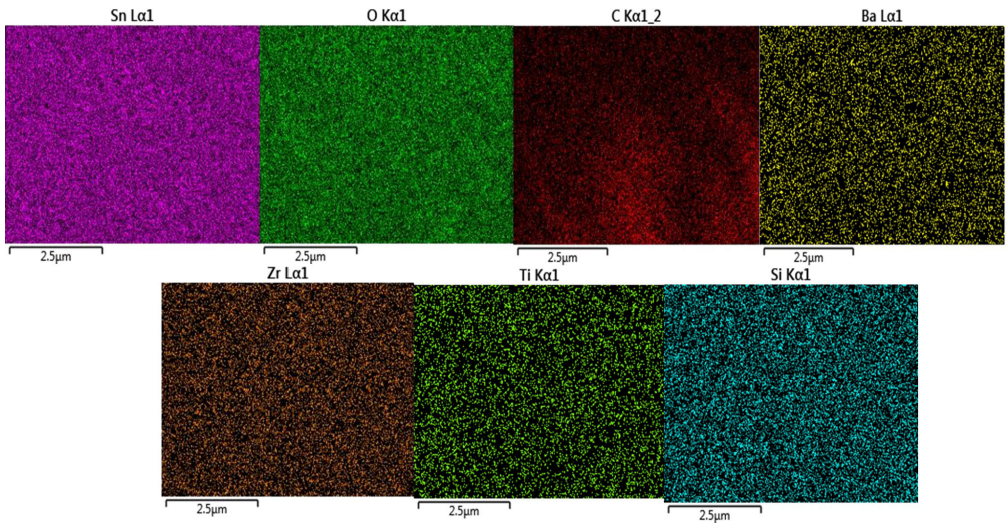

Figure 5. Mapping of BT-BZT elements at annealing temperatures of 700 °C, 750 °C, and 800 °C.

visible region. A higher absorbance in BT-BZT thin film greater photon energy aborption as light passed through the material. The UV-Vis spectrum further provides insight into the band gap energy of the sample, which was determined using the Kubelka-Munk equation or the remission function *F(R)*[18]. The estimated band gap energies for samples annealed at 700 °C, 750 °C, and 800 °C were approximately 3.80 eV, 3.70 eV, and 3.50 eV, respectively. As depicted in Figure 7, the band gap decreases as the annealing temperature increases. This reduction is attributed to the temperature increase leading to an expansion in the spacing between atoms. As the annealing temperature increases, the crystal structure tends to become closer and more compact, leading to a reduction in the resulting energy band gap[19].

Figure 8 presents the Nyquist plot of the impedance spectroscopy measurement data. This plot illustrates. the correlation between imaginary and real impedance, depicted as a semicircular graph. This semicircle indicates the presence of polarization within the grains. The plot of *Z*'' against *Z*' also reveals variations in the diameter of the semicircle, which diminishes as the annealing temperature rises. This suggests a decrease in material resistivity with

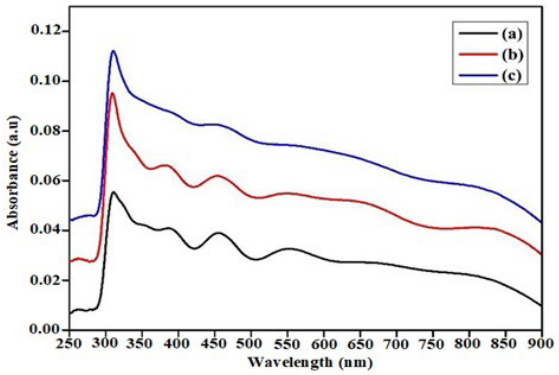

Figure 6. Absorbance spectrum of BT-BZT samples annealed at (a) 700 °C, (b) 750 °C, and (c) 800 °C for 1 hour.

increasing annealing temperature, implying a concurrent increase in conductivity[20].

High annealing temperatures increase the grain size of the material through a more active atomic diffusion process. Grain boundaries usually act as obstacles to electrical conductivity because they have high energy and often contain many defects. As the number of grain boundaries decreases due to grain growth, the path of charge movement becomes smoother, resulting in decreased resistivity[21,22]. Good conductivity implies good dielectric properties[23]. From the Nyquist plot, an equivalent series circuit representing the relationship between *Z*'' and *Z*' was obtained, as shown in Figure 8. Table 2 shows the parameters of the equivalent electric circuit.

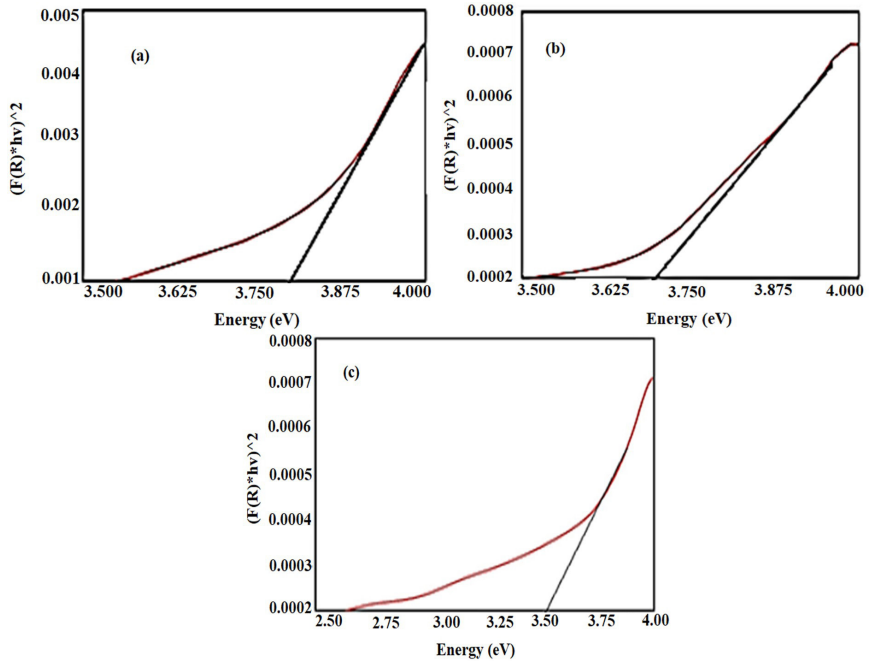

Figure 7. Calculation of the energy band gap (Eg) was carried out using the relationship $((R).hv)^2$ and energy (eV) at three different temperatures: (a) 700 °C, (b) 750 °C, and (c) 800 °C.

Table 2. Parameters of the equivalent electric circuit.

Sample	Parameters	Values of the Parameters	Errors, %
BT-BZT700	C1	4.8188E-09	0.38918
	R1	54.535	0.15785
	R2	4.5184	2.4218
	P1	1.0118E-11	###
	n1	0.75798	75.545
BT-BZT750	C1	4.8036E-10	14.479
	C2	7.8535E-09	0.89439
	R1	29.685	1.0406
	R2	4.1841	15.167
BT-BZT800	C1	3.6057E-14	###
	C2	1.012E-08	0.79475
	R1	22.395	0.89622
	R2	4.4232	12.539

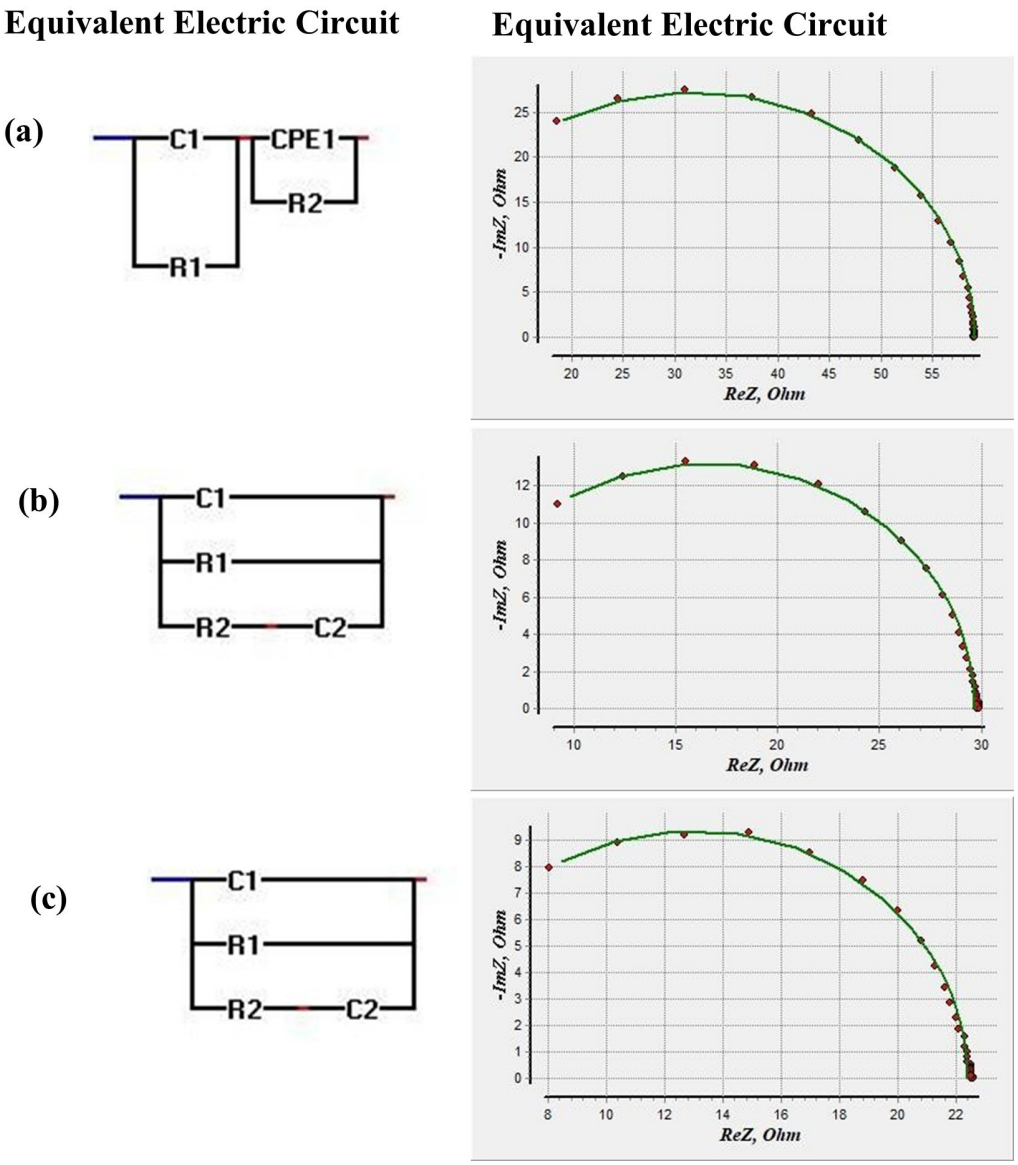

Figure 8. The relationship of Z'' and Z' and equivalent circuits representing various annealing temperatures of (a) 700 °C (b) 750 °C, and (c) 800 °C.

Figure 9 shows a decrease in capacitance as frequency increases, which complies with theoretical predictions. This trend reflects an inversely proportional relationship between capacitance and frequency, based on AC voltage principles[24]. The annealing temperature also affects the capacitance of the BT-BZT material. At an annealing temperature of 700 °C, FESEM analysis reveals fewer grain formations. These grains decrease the resistivity and increase the conductivity of the sample[25]. The resistivity decreases as the annealing temperature increases due to the formation of grains.

Figure 10 illustrates that increasing the annealing temperature leads to a higher lattice density, which in turn enhances the material's dipole moment. A high number of dipoles contributes to high polarization. Polarization is

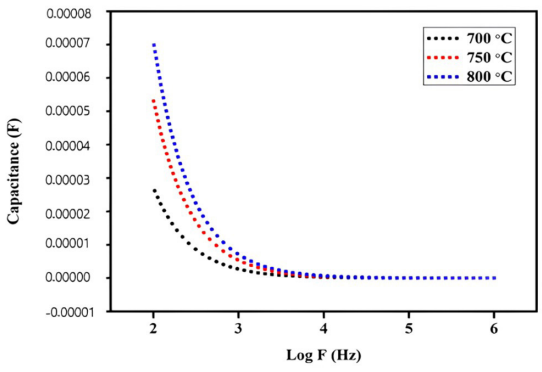

Figure 9. Relationship of capacitance (F) to log frequency (Hz) with variations in annealing temperature: 700 °C, 750 °C, and 800 °C.

Table 3. Capacitance values, dielectric constant at a frequency of 100Hz and 1MHz at the sample of BT-BZT annealed at the temperature of 700, 750 and 800 °C.

Sample	Capacitance (F)	Dielectric constant	Frequency
BT-BZT700	(Max) 2.7 ×10^{-5}	(Max) 30513.02	100 Hz
	(Min) 5.24 ×10^{-9}	(Min) 3.6329	1 MHz
BT-BZT750	(Max) 5.34 ×10^{-5}	(Max) 60303.90	100 Hz
	(Min) 1.11 ×10^{-8}	(Min) 12.5321	1 MHz
BT-BZT800	(Max) 7.08 ×10^{-5}	(Max) 79951.95	100 Hz
	(Min) 1.41 ×10^{-8}	(Min) 15.9305	1 MHz

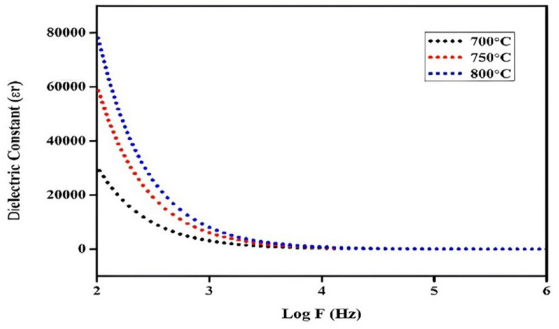

Figure 10. Relationship of dielectric constant ε_r to log Frequency (Hz) with various annealing temperatures of 700 °C, 750 °C and 800 °C.

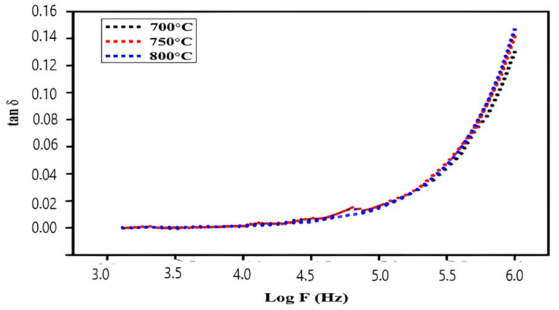

Figure 11. Relationship of tan δ to Frequency with various annealing temperatures of 700 °C, 750 °C and 800 °C.

directly proportional to the dielectric constant of a dielectric material[26]. Thus, samples treated at higher temperatures demonstrated a higher dielectric constant, making them suitable as building blocks for capacitors. A high dielectric constant value indicates that the capacitor can withstand high temperatures[1].

Figure 11 shows that the dielectric loss increases with annealing temperature. At 800 °C, the electric loss reaches a maximum of approximately 0.14 compared to 0.13 at 750 °C, and 0.12 at 700 °C. An increase in annealing temperature leads to an increase in dipoles, resulting in higher resistance and increased dielectric loss[27]. The energy lost by the material is converted into heat, which arises due to material resistance[28]. Table 3 shows the capacitance values and dielectric constant at frequencies of 100 Hz and 1 MHz.

4. Conclusions

Annealing temperature affects the capacitance of the BT-BZT material. Higher annealing temperatures result in fewer grains. An annealing temperature of 800 °C demonstrated fewer grains, as observed in the FESEM results. The grains formed decreased the resistivity and increased the conductivity, with an energy band gap (*Eg*) of ~3.50 eV. A material with good conductivity enhances the capacitance value of the dielectric materials of the capacitor. For the annealing temperature of 800 °C, the produced capacitance value was approximately 70 µF at a frequency of 100 Hz. The corresponding dielectric constant was around 80,000, with a dielectric loss tangent (tan δ) of approximately 0.14. The increase in annealing temperature improved the crystallinity of the BT-BZT material. The rise in temperature increases lattice density, increasing the dipole moment in the material. A high number of dipoles leads to a higher value of polarization. Polarization is directly proportional to the dielectric constant of a dielectric material. Thus, samples annealed at 800 °C exhibit a high dielectric constant, making them suitable as a building block for high-temperature capacitors.

5. Acknowledgments

Rahmi Dewi acknowledges the financial support from the collaboration between the National Research Agency (BRIN), the Education Fund Management Institute (LPDP), and the University of Riau Research and Community Service Institute (LPPM) number 82/II.7/ HK/2022. Rahmi Dewi also acknowledges that a preprint of this works has previously been published[29].

6. References

1. Shen Z, Wang X, Li L. Dielectric properties and microstructures of Ta-doped $BaTiO_3$–$(Bi_{0.5}Na_{0.5})$ TiO_3 ceramics for X9R applications. J Mater Sci Mater Electron. 2016;28(4):3768-73. http://doi.org/10.1007/s10854-016-5986-z.
2. Yao JG, Wang X, Gong H, Wen H, Li L. Nb-doped $BaTiO_3$-$(Bi_{0.5}Na_{0.5})TiO_3$ ceramics with core-shell structure for high-temperature dielectric applications. Appl Phys. 2011;50:1502.
3. Ren XH, Gui DY. Structure and dielectric behavior of Yb_2O_3-MgO Co-doped 0.92$BaTiO_3$- 0.08$(Na_{0.5}Bi_{0.5})TiO_3$ ferroelectric relaxor. Materials. 2021;14(22):6802. http://doi.org/10.3390/ma14226802. PMid:34832202.
4. Li L, Wang M, Liu Y, Chen J, Zhang N. The effect of glass addition on the ultra - broad temperature stability of $BaTiO_3$–$Na_{0.5}Bi_{0.5}TiO_3$–Nb_2O_5-based ceramics. Int. 2014;40:1105-10.

5. Lee WH, Su CY. Improvement in the temperature stability of a $BaTiO_3$-based multilayer ceramic capacitor by constrained sintering. J Am Ceram Soc. 2007;90(10):3345-8. http://doi.org/10.1111/j.1551-2916.2007.01900.x.
6. Antonelli E, Letonturier M, M'Peko JC. Microstructural, Structural and Dielectric Properties of Er^{3+}-Modified $BaTi_{0.85}Zr_{0.15}O_3$ Ceramics. J Eur Ceram Soc. 2009;29(8):1449-55. http://doi.org/10.1016/j.jeurceramsoc.2008.09.009.
7. Lu H-Y, Bow J-S, Deng W-H. Core-shell structures in ZrO_2-modified $BaTiO_3$ ceramic. J Am Ceram Soc. 1990;73(1):3562-8. http://doi.org/10.1111/j.1151-2916.1990.tb04258.x.
8. Dewi R, Luqman TS, Sitorus SN, Vitayaya O, Rini AS, Zuhdi A. The effect of annealing temperature on microstructure and energy band gap of $0.2BaTiO_3 - 0.8BaZr_{0.5}Ti_{0.5}O_3$ nano material. Mater Today Proc. 2023;87:159-63. http://doi.org/10.1016/j.matpr.2023.02.391.
9. Sangiorgi A, Aversa L, Tatti R, Verucchi R, Sanson A. Spectrophotometric method for optical band gap and electronic transitions determination of semiconductor materials. Opt Mater. 2017;64:18-25. http://doi.org/10.1016/j.optmat.2016.11.014.
10. Hidayat T, Dewi R, Hamzah Y. Effect of holding time on optical structure properties of $Ba(Zr_{0.5}Ti_{0.5})O_3$ thin film using sol-gel method. Sci Technol Commun J. 2021;1(2):59-68. http://doi.org/10.59190/stc.v1i2.28.
11. Jia W, Hou Y, Zheng M, Xu Y, Zhu M, Yang K, et al. Advances in lead-free high-temperature dielectric materials for ceramic capacitor application. IET Nanodielectr. 2018;1(1):3-16. http://doi.org/10.1049/iet-nde.2017.0003.
12. Han J, Yin J, Wu J. BNT-based ferroelectric ceramics: electrical properties modification by Ta_2O_5 oxide addition. J Am Ceram Soc. 2020;103(1):412-22. http://doi.org/10.1111/jace.16752.
13. Lahure P, Salunke P, Soliwal R, Yadav A, Tripathi S, Koser AA. X-ray diffraction study of ZnO nanoparticles. Int J Sci Res Phys Appl Sci. 2015;3(1):32-3.
14. Gbashi KR, Bahari A, Lafta SH. Thin films for nano-elektronics applications based on $BaCaTiO_3$-$SrZnTiO_3$ perovskite with Au electrodes. Appl Phys, A Mater Sci Process. 2023;129(5):350. http://doi.org/10.1007/s00339-023-06621-1.
15. Chi Q, Liu G, Zhang C, Cui Y, Wang X, Lei Q. Microstructure and dielectric properties of BZT-BCT/PVDF nanocomposites. Results Phys. 2017;8:391-6. http://doi.org/10.1016/j.rinp.2017.12.052.
16. Wang H, Li Q, Jia Y, Yadav AK, Yan B, Shen Q, et al. Enhanced dielectric temperature stability and energy-storage properties of $(Y_{0.5}Nb_{0.5})^{4+}$ co-doped $(Bi_{0.5}Na_{0.5})0.94Ba_{0.06}TiO_3$ lead-free relaxor ceramics. J Mater Sci. 2021;56(26):14672-83. http://doi.org/10.1007/s10853-021-06193-6.
17. Chiyah B, Kayed K. Effect of annealing temperature on the structural and optical properties of silver oxide thin films prepared by thermal evaporation with subsequent annealing. Int J Nanoelectron Mater. 2018;11(3):307-12.
18. Xin JZ, Leung CW, Chan HLW. Composition dependence of structural and optical properties of $Ba(Zr_x,Ti_{1-x})O_3$ thin films grown on MgO substrates by pulsed laser deposition. Thin Solid Films. 2011;519(19):6313-8. http://doi.org/10.1016/j.tsf.2011.04.007.
19. Tesfaye Jule L, Ramaswamy K, Bekele B, Gungure AS. Experimental investigation on the impacts of annealing temperatures on titanium dioxide nanoparticles structure, size and optical properties synthesized through sol-gel methods. Mater Today Proc. 2021;45:5752-8. http://doi.org/10.1016/j.matpr.2021.02.586.
20. Das SN, Pardhan SK, Bhuyan S, Sahoo S, Choudhary RNP, Goswami MN. Dielectric and impedance characteristics of nickel-modified $BiFeO_3$. J Electron Mater. 2018;47(1):843-54. http://doi.org/10.1007/s11664-017-5848-3.
21. Bishara H, Lee S, Brink T, Ghidelli M, Dehm G. Understanding grain boundary electrical resistivity in Cu: the effect of boundary structure. ACS Nano. 2021;15(10):16607. http://doi.org/10.1021/acsnano.1c06367. PMid:34605639.
22. Ma G, Sheng J, Gao Y, Tuo L, Li Y, La P. Effect of annealing temperature on microstructure and mechanical properties of 00Cr21CuTi stainless steel cold-rolled sheets. Metals. 2024;14(12):1367. http://doi.org/10.3390/met14121367.
23. Ahmad MM, Alismail L, Alshoaibi A, Aljaafari A, Kotb HM, Hassanien R. Dielectric behavior of spark plasma sintered $BaTi_{0.7}Zr_{0.3}O_3$ relaxor ferroelectrics. Results Phys. 2019;15:102799. http://doi.org/10.1016/j.rinp.2019.102799.
24. Hemeda M, Salem BI, Mostafa M. Structural and electric properties of strontium barium titanate prepared by tartrate precursor method. Eur Phys J Plus. 2020;135(1):46. http://doi.org/10.1140/epjp/s13360-019-00021-2.
25. Thanachayanont M, Yordsri V, Kijamnajsuk S, Binhayeeniyi N, Muensit N. Microstructural investigation of sol-gel BZT powders. Mater Lett. 2012;82:205-7. http://doi.org/10.1016/j.matlet.2012.05.075.
26. Dewi R, Krisman K, Zuhdi Z, Rini AS, Hussains T. View of characteristic making of $Ba_{0.4}Sr_{0.6}TiO_3$ thin film nanoparticle. Trends in Sciences. 2022;19(19):6178. http://doi.org/10.48048/tis.2022.6178.
27. Sangwan KM, Ahlawat N, Kundu RS, Suman R, Sunita R, Ahlawat N, et al. Improved dielectric and ferroelectric properties of Mn doped barium zirconium titanate (BZT) ceramics for energy storage applications. J Phys Chem Solids. 2018;117:158-66. http://doi.org/10.1016/j.jpcs.2018.01.051.
28. Abomostafa HM, El-Komy GM, Turky GM. Microstructure and dielectric study of pure BST and doped BSTF ceramic materials by broadband dielectric spectroscopy. Curr Appl Phys. 2020;20(5):611-8. http://doi.org/10.1016/j.cap.2020.02.011.
29. Dewi R, Luqman TS, Sitorus SN, Vitayaya O, Rini AS, Hamzah Y. Microstructure, optical properties and dielectric properties of thin film ceramics $BaTiO_3$–$BaZr_{0.5}Ti_{0.5}O_3$ for high temperature capacitor, SSRN. 2023. In press. http://doi.org/10.2139/ssrn.4469068.

Data Availability

All data generated or analyzed during this study are included in this published article.